


Stability and quantum escape dynamics of spin-orbit-coupled Bose-Einstein condensates in the shallow trap

Yan-Chao Zhang, Yue Jian, Zi-Fa Yu, Ai-Xia Zhang, and Ju-Kui Xue ^{*}

College of Physics and Electronics Engineering, Northwest Normal University, Lanzhou 730070, China



(Received 22 January 2020; accepted 4 September 2020; published 28 September 2020)

The Bose-Einstein condensates in a finite depth potential well provide an ideal platform to study the quantum escape dynamics. In this paper, the ground state, tunneling, and diffusion dynamics of the spin-orbit coupling (SOC) of Bose-Einstein condensates with two pseudospin components in a shallow trap are studied analytically and numerically. The phase transition between the plane-wave phase and zero-momentum phase of the ground state is obtained. Furthermore, the stability of the ground state is discussed, and the stability diagram in the parameter space is provided. The bound state (in which condensates are stably trapped in the potential well), the quasibound state (in which condensates tunnel through the well), and the unstable state (in which diffusion occurs) are revealed. We find that the finite depth potential well has an important effect on the phase transition of the ground state, and, interestingly, SOC can stabilize the system against the diffusion and manipulate the tunneling and diffusion dynamics. In particular, spatial anisotropic tunneling and diffusion dynamics of the two pseudospin components induced by SOC in quasibound and unstable states are observed. We provide an effective model and method to study and control the quantum tunneling and diffusion dynamics.

DOI: [10.1103/PhysRevE.102.032220](https://doi.org/10.1103/PhysRevE.102.032220)

I. INTRODUCTION

Spin-orbit coupling (SOC) represents a major source of magnetic interaction which involves the fine structure in atomic physics. SOC also plays a crucial role in solid materials, such as topological insulator [1,2], spintronic devices [3], spin Hall effects [4–7], and quantum computation [8]. In a cold atomic system, we aim at the neutral atoms, which cannot experience the spin-orbit coupling naturally and it therefore has to be engineered. SOC can be induced by Raman lasers in this case. Then the hyperfine structure (playing a role of the quasi-spin-up and -down states) is involved for cold atoms because of the Raman coupling between the hyperfine ground states [9,10]. It becomes indispensable in many ultracold gases with the experimental realization of SOC with equal Rashba [11] and Dresselhaus [12] contributions, especially Bose-Einstein condensates (BECs) [13,14]. It has been shown that spin-orbit coupled Bose-Einstein condensates (SOC-BECs) can be generated by two counter-propagating Raman lasers, and most experimental parameters can be controlled by optic or magnetic means [15,16]. SOC-BECs exhibit many interesting localized phenomena, such as solitons [17–20], gap solitons [21–23], and vortex structure [24,25]. In particular, many quantum ground-state phases have been investigated, such as the zero-momentum phase, the plane-wave phase, and the stripe phase [13–15,25–30]. Interestingly, it is found that SOC can maintain the system's stability with stable soliton-like localized phenomena in a purely attractive SOC-BEC in free space, and it is also observed that SOC can stabilize the system against collapse [31–34].

Furthermore, the anisotropic expansion dynamics induced by SOC is revealed in free space [35,36]. Usually, infinite depth harmonic potential is employed to trap the BECs. The condensates can be trapped stably or get collapsed in this potential well with different states. Correspondingly, the studies of the ground state and the stability of the SOC-BECs are focused on the case of free space or an infinite depth harmonic potential well.

Different from the case of the infinite depth potential well, there is a metastable state (quasibound state) for atoms in the finite depth potential well, where tunneling occurs [37–40]. Tunneling is of great significance to quantum physics and chemistry and much work have been reported, such as imaging of materials [41] and tunneling lifetime, which can be controlled by varying the depth of the shallow trap [42]. Tunneling is vital to the quantum transport and the corresponding quantum well structure. Thus, deep study and understanding of the tunneling dynamics are still an open question. Because of the highly controllability of atomic interaction and trap geometries, an atomic condensate in the shallow trap provides an ideal platform to explore the quantum tunneling dynamics [43–45]. However, the previous studies on the tunneling dynamics of the atomic condensates in the shallow trap do not take the SOC into account, and the pseudospin component of the system is simple. The influence of SOC on the ground-state phase transition, the stability of the ground state, and the tunneling dynamics with two pseudospin components in the shallow trap are not clear. We expect that rich quantum escape dynamics will occur in SOC-BECs.

In this paper, the ground state and the stability of the SOC-BECs with two pseudospin components trapped in the finite depth potential well are studied using the variational method and numerical simulation. The phase transition of the

^{*}Corresponding author: xuejk@nwnu.edu.cn

ground state and the stability of the ground state are analyzed. The stable bound state, the quasibound state, and the unstable diffusion state are revealed. It is shown that the parameter of the finite depth potential well, atomic interactions, spin-orbit coupling, and Raman coupling have strong coupling effects on the ground state. The effect of the finite depth potential on the phase transition depends on intraspecies and interspecies interactions. When the intraspecies interaction is greater (smaller) than the interspecies interaction, the finite depth potential well suppresses (promotes) the transformation of the system from zero-momentum phase into plane-wave phase. The effect of the finite depth potential well on phase transition disappears when intraspecies and interspecies interactions are equal. Interestingly, spin-orbit coupling (Raman coupling) can stabilize (destabilize) the system against diffusion and manipulate the transition of the system between the bound state, quasibound state (tunneling state), and unstable diffusion state. Moreover, the intuitive proof of this phenomenon is provided. Furthermore, the tunneling and diffusion dynamics in quasibound and unstable states are discussed, and the spatial anisotropic tunneling and diffusion dynamics induced by spin-orbit coupling are observed.

The paper is organized as follows. In Sec. II the model and the variational analysis of the system's ground state are provided. In Sec. III the phase transition of the ground state is discussed. In Sec. IV the stability of the ground state is discussed. In Sec. V the tunneling and diffusion dynamics of the system are discussed. In Sec. VI stability (instability) induced by SOC (Raman coupling) are demonstrated intuitively. Section VII is a brief summary.

II. THE MODEL AND VARIATIONAL ANALYSIS

We consider the ^{87}Rb atom with total angular momentum $F = 1$ and spin $J = 1/2$. First, a magnetic field is applied to split the degeneracy of the ground state into $|1, 1\rangle$, $|1, 0\rangle$, and $|1, -1\rangle$ states. The $|1, 1\rangle$ state is far detuned from the remaining two states, thus the $|1, 1\rangle$ state is neglected [13]. Then the Raman lasers effectively couple the $|1, 0\rangle$ and $|1, -1\rangle$ states. We label $|1, 0\rangle$ and $|1, -1\rangle$ as two pseudospin states in analogy with an electron's two spin states. From $|\psi_1\rangle = |1, 0\rangle$ and $|\psi_2\rangle = |1, -1\rangle$, the SOC-BECs with two pseudospin components can be characterized by $\Psi = (\psi_1, \psi_2)^T$ (hereafter the superscript T stands for the transposition), and a one-dimensional symmetric finite depth potential well is employed to trap the condensates (see Fig. 1). The dimensionless Hamilton describing the system has the following form [37–39,45–50]:

$$H = H_{\text{SOC}} + G, \quad (1)$$

and the physical variables are rescaled as $\Psi \sim \sqrt{a_0}\Psi$, $x \sim a_0x$, where $a_0 = \sqrt{\hbar/m\omega_0}$ is the characteristic length along the x direction, m is the mass of the atom, and ω_0 is the trapping frequency along the x direction. The dimensionless single-particle Hamiltonian is

$$H_{\text{SOC}} = -\partial^2/\partial x^2 - ik_L\sigma_z\partial/\partial x + \Omega\sigma_x + V(x). \quad (2)$$

After the pseudospin rotation, H_{SOC} including $p_x\sigma_z$ corresponds to an equal weight mixing of Rashba and Dresselhaus coupling [10,14,26,48]. The $k_L = \tilde{k}_L/(2\hbar a_0^{-1})$ is the dimen-

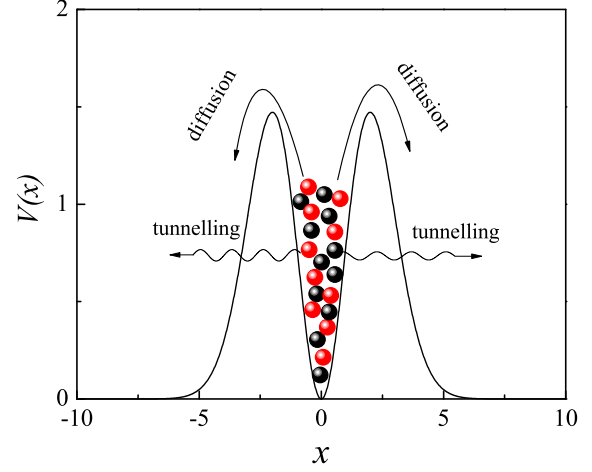


FIG. 1. The sketch of the model. $c = 0.1$.

sionless strength of the SOC, and $\Omega = \tilde{\Omega}/(2\hbar\omega_0)$ is the dimensionless Raman coupling. σ_x and σ_z are the standard 2×2 Pauli matrices. $V(x) = x^2 e^{-cx^2}$ is the dimensionless shallow trap, which is shown in Fig. 1. This special finite depth potential well can be generated by multiplying the broad Gaussian envelopes generated by the waist of the trapping laser beam and the central harmonic potential generated by a second, more narrowly focused laser beam, or by a higher Hermite-Gauss mode of the laser as used in creating BECs' wave guides, or by a laser beam with embedded vorticity induced by passing the beam through a phase mask [39]. With the increasing c , the trap is weakened, otherwise it is strengthened, and the depth and width of the $V(x)$ are both governed by c . In this paper, we mainly discuss the comprehensive influence of this parameter on the system. G is a 2×2 matrix describing the two-body interaction under the mean-field approximation, where

$$G = \text{diag}(g_{11}|\psi_1|^2 + g_{12}|\psi_2|^2, g_{22}|\psi_2|^2 + g_{12}|\psi_1|^2); \quad (3)$$

$g_{ii} = 4a_{ii}N\hbar/m\omega_0 l_{\perp}^2 a_0$ and $g_{ij} = 4a_{ij}N\hbar/m\omega_0 l_{\perp}^2 a_0$ represent the dimensionless intra-species and interspecies interaction, respectively. N denotes the total number of atoms, and a_{ij} and a_{ii} are the intraspecies and interspecies s-wave scattering length. $l_{\perp} = \sqrt{\hbar/m\omega_{\perp}}$ is the characteristic length in the longitudinal plane with its trapped frequency ω_{\perp} . We set $g_{11} = g_{22} = g$ in this paper owing to neglecting the Zeeman fields effects.

In order to investigate the ground state of the system, the variational method is used, and the trial wave function with Gaussian form can be provided [38]:

$$\Psi(x, t) = \begin{pmatrix} \psi_1 \\ \psi_2 \end{pmatrix} = \frac{1}{\sqrt{2}} \begin{pmatrix} e^{\frac{i\phi}{2}\sqrt{1+s}} \\ -e^{-\frac{i\phi}{2}\sqrt{1-s}} \end{pmatrix} \times \frac{e^{-\frac{x^2}{2R^2} + ipx}}{(\sqrt{\pi}R)^{\frac{1}{2}}}. \quad (4)$$

The trial wave function is normalized, i.e., $\int [\psi_1^* \psi_1 + \psi_2^* \psi_2] dx = 1$. p and R are the momentum and width of the wave packets, respectively, s ($-1 \leq s \leq 1$) is the expectation

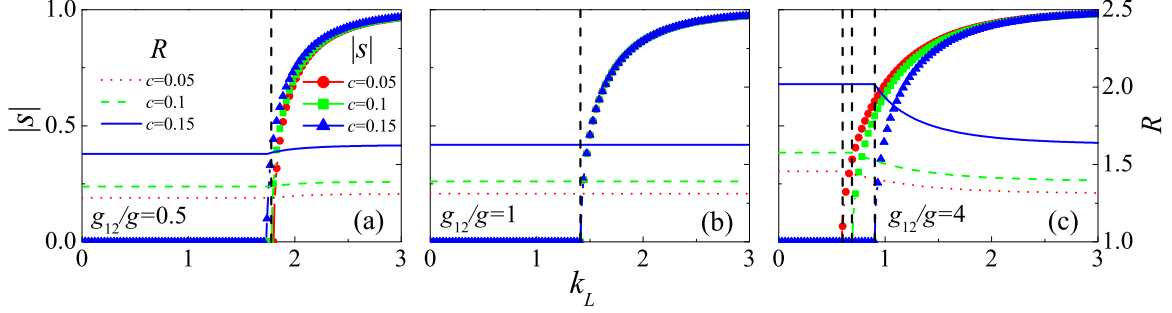


FIG. 2. The corresponding equilibrium s and R in the ground state against k_L under different c . We set $g = 1$ and $\Omega = 1$.

value of the spin, and ϕ is the phase difference between the two pseudospin components.

We can obtain the energy of the system by $E = \int [\Psi^* H_{SOC} \Psi + \frac{1}{2} \Psi^* G \Psi] dx$:

$$E = p^2 + \frac{1}{2R^2} + \frac{R^2}{2(1+cR^2)^{\frac{3}{2}}} + k_L s p - \Omega \sqrt{1-s^2} \cos \phi + \frac{g+g_{12}+(g-g_{12})s^2}{4\sqrt{2\pi}R}. \quad (5)$$

Using $\frac{\partial E}{\partial q_i} = 0$, where $q_i = R, s, \phi, p$, the ground-state solutions are obtained, $\phi = 0$, and

$$p = -\frac{1}{2} k_L s, \quad (6)$$

$$\frac{1}{R^3} + \frac{3cR^2}{2(1+cR^2)^{\frac{5}{2}}} + \frac{g+g_{12}+(g-g_{12})s^2}{4\sqrt{2\pi}R^2} = \frac{R}{(1+cR^2)^{\frac{3}{2}}}, \quad (7)$$

$$s f = 0, \left(f = k_L^2 - \frac{g-g_{12}}{\sqrt{2\pi}R} - \frac{2\Omega}{\sqrt{1-s^2}} \right). \quad (8)$$

R and s can be obtained by solving Eqs. (7) and (8), in which the solution with the minimum energy represents the ground state of the system. When the system is in the ground state, R is a finite width, and different ground-state phases depending on s occur.

III. THE GROUND-STATE PHASE DIAGRAM

The ground state exists when Eqs. (7) and (8) have real solutions. Meanwhile, $s = 0$ represents the zero-momentum phase without spin polarization and $s \neq 0$ represents the plane-wave phase with spin polarization. Here we focus on only the phase transition between the zero-momentum phase and the plane-wave phase.

Figure 2 shows the numerical solution of the stationary width for the wave packet R and expectation value of the spin s against the strength of SOC under different interspecies interaction g_{12}/g and parameter c (we set $g = 1$ and $\Omega = 1$). There is a critical value k_{LC} that s remains at 0 for $k_L < k_{LC}$ (condensates are in a zero-momentum phase), while s increases with increasing k_L for $k_L > k_{LC}$ (condensates are in a plane-wave phase), where

$$k_{LC} = \sqrt{(g-g_{12})/\sqrt{2\pi}R + 2\Omega}, \quad (9)$$

and k_{LC} is the phase transition point determined by $f = 0$ and $s = 0$. Correspondingly, R keeps unchanged for $k_L < k_{LC}$ due to decoupling between s and R ; however, R changes with k_L for $k_L > k_{LC}$. Interspecies repulsion widens the ground-state width R . The increase of c weakens the potential well and leads to a broadening of R , i.e., R increases with increase of g_{12} and decrease of c . Furthermore, R is positively correlated with the strength of SOC when $g_{12}/g < 1$ [see Fig. 2(a)], i.e., R increases with the increase of k_L for $k_L > k_{LC}$, while R is negatively correlated with the strength of SOC when $g_{12}/g > 1$ [see Fig. 2(c)], i.e., R decreases with the increase of k_L for $k_L > k_{LC}$. In particular, R remains invariable with the change of k_L when $g_{12}/g = 1$ is satisfied [see Fig. 2(b)]. Interestingly, the variation of R against SOC k_L is continuous, but the slope is discontinuous at the phase transition point, and this corresponds to a second-order phase transition when $g_{12}/g \neq 1$. In addition, we can see the phase transition point k_{LC} increases with c when $g_{12}/g > 1$, while c has a weak influence on k_{LC} when $g_{12}/g \leq 1$. Those are further clarified in Fig. 3.

To explore the phase transition in the ground state more comprehensively, we make the phase diagram in the (Ω, k_L) plane under different parameter of the potential well c and interspecies repulsion g_{12}/g [see Figs. 3(a)–(d)]. For a fixed

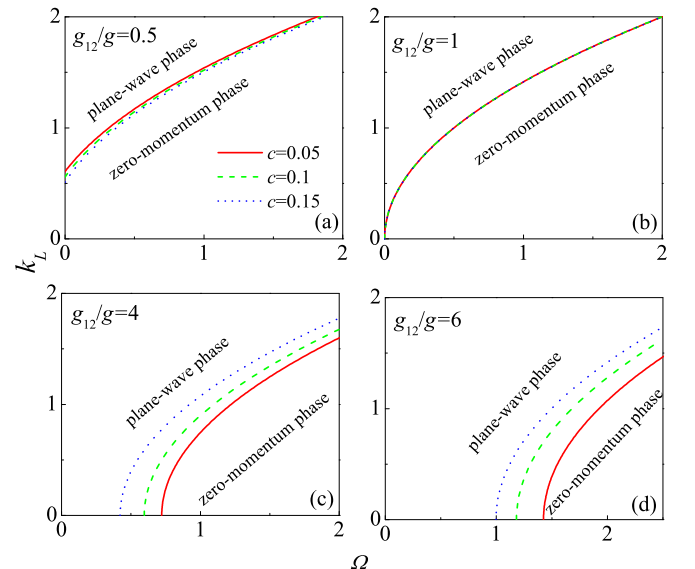


FIG. 3. Phase diagram in (Ω, k_L) plane under different c and g_{12}/g . We set $g = 1$.

g_{12}/g (we set $g = 1$), condensates transfer from the zero-momentum phase into the plane-wave phase with the increase of k_L and decrease of Ω . Phase transition curves integrally shift right when interspecies repulsion is enhanced, i.e., the plane-wave phase expands to a larger Ω region with the increase of g_{12}/g . When $g_{12}/g = 1$, the effect of c on the phase transition disappears completely [see Fig. 3(b)]. However, Figs. 3(c)–3(d) illustrate that increasing c suppresses the condensates transforming from the zero-momentum phase into plane-wave phase when $g_{12}/g > 1$, and the suppression becomes more significant for large interspecies repulsion. Thus, for SOC, the parameter of the potential well and interspecies interaction can be adjusted to design the ground-state structures of the condensates.

IV. THE STABILITY OF THE GROUND STATE

Condensates cannot be trapped in the potential well when parameter c becomes large enough (the finite depth potential well tends to the situation of the free space), and condensates enter into the unstable state where diffusion occurs with intraspecies repulsion. In this case, Eqs. (7) and (8) do not have real solutions. Sufficiently small c corresponds to the potential well of infinite depth, where condensates are trapped in the well stably. Between the two extremes, i.e., for the finite depth potential well, there is a metastable state (i.e., quasibound state) where tunneling occurs. We can divide the ground state into a bound state and quasibound state by the chemical potential,

$$\mu = \int (\psi_1^*, \psi_2^*) H(\psi_1, \psi_2)^T dx, \quad (10)$$

where μ is the chemical potential of the condensates. Inserting equilibria R, p, s, ϕ into Eq. (10), one obtains the chemical potential of the ground state,

$$\begin{aligned} \mu = & \frac{R}{2(1+cR^2)^{\frac{3}{2}}} - \frac{1}{4}k_L^2s^2 + \frac{1}{2R^2} - \Omega\sqrt{1-s^2} \\ & + \frac{(g+g_{12}) - (g-g_{12})s^2}{2\sqrt{2\pi}R}. \end{aligned} \quad (11)$$

The trapping potential $V(x) \rightarrow 0$ when $x \rightarrow \infty$ (see Fig. 1), i.e., the background potential is 0. Then, when the chemical potential is stronger than the background potential (chemical potential $\mu > 0$), i.e., the chemical potential is positive, the atoms can tunnel outside the finite depth potential well, and the condensates are in the quasibound state in this case. When the chemical potential of the condensates is weaker than the background potential ($\mu < 0$), i.e., the chemical potential is negative, it is impossible for atoms to escape outside the potential well, and the condensates are in the bound state in this case. Thus, the transition from the quasibound to bound state occurs when the ground-state chemical potential μ changes the sign from positive to negative [38]. Therefore, by combining stationary equations (7) and (8) and the ground-state chemical potential from Eq. (11), the g - c plane is divided into three regions (see Fig. 4): the unstable state (i.e., diffusion state), bound state, and quasibound state (i.e., tunneling state).

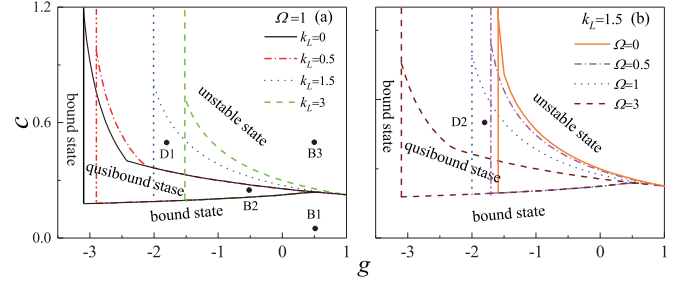


FIG. 4. Stability phase diagram in the g - c plane, (a) with different strength of SOC k_L under Raman coupling $\Omega = 1$, and (b) with different Ω under $k_L = 1.5$. We set $g_{12} = 1$.

Figure 4 is the stability phase diagram in the g - c plane for different k_L and Ω . It illustrates, for the fixed k_L and Ω , when c increases (the trap is weakened), the stability can be maintained by reducing the interspecies repulsion or increasing the intraspecies attractive. Figure 4(a) shows that, with the increase of k_L , the regions of bound and quasibound states expand to the weak attractive intraatomic interaction region and even to the weak repulsive intra-atomic interaction region for the larger c case under the fixed Ω ; i.e., SOC can balance the mean-field repulsion to prevent the condensates against the diffusion. However, when k_L is large enough ($k_L > 3$), the influence of k_L on the stability diagram is inhibited. The system enters into the fully polarized plane-wave phase for the fixed Ω with large k_L , s tends to 1 and hardly changes (see Fig. 2), and Eq. (7) related to the stability is independent on s and k_L in this case. Figure 4(b) shows that, for the fixed k_L with increasing Ω , the regions of the unstable state expand to the strong attractive intra-atomic interaction region, i.e., Raman coupling promotes the diffusion of the condensates. Thus, strong SOC (or weak Raman coupling) can stabilize the system and manipulate the transition of the system between the bound state, quasibound state, and unstable diffusion state. As marked by point $D1$ ($D2$) in Fig. 4(a) [Fig. 4(b)], the condensates experience the diffusion state in the zero-momentum phase (bound state in the plane-wave phase), quasibound state in the plane-wave phase, and bound state in the plane-wave phase (diffusion state in the zero-momentum phase) transitions successively with the increase of k_L (Ω) under the fixed Ω (k_L). In addition, when c is sufficiently small (the depth of the potential well tends to infinite) and the atomic-repulsion is large enough, the potential well loses the property of finite depth, i.e., the quasibound state disappears, and in this case, condensates transfer from the stable bound state to unstable diffusion state directly (see Fig. 4). Moreover, Fig. 4 appears as a sharp corner between the quasibound state and the bound state for negative g and small c region; it could be explained that the width of the ground-state wave packets become smaller than the width of the trap as attractive interactions are increased or the trapping ability of the potential well is weakened, and therefore the trap has a weak effect on the energy of the system. Similarly, when the attractive intraspecies interaction reaches a certain value, the system is all stable under arbitrary value of c as shown in Fig. 4. Sufficiently strong attractive interactions result in the much narrower wave packets, which are far smaller than the

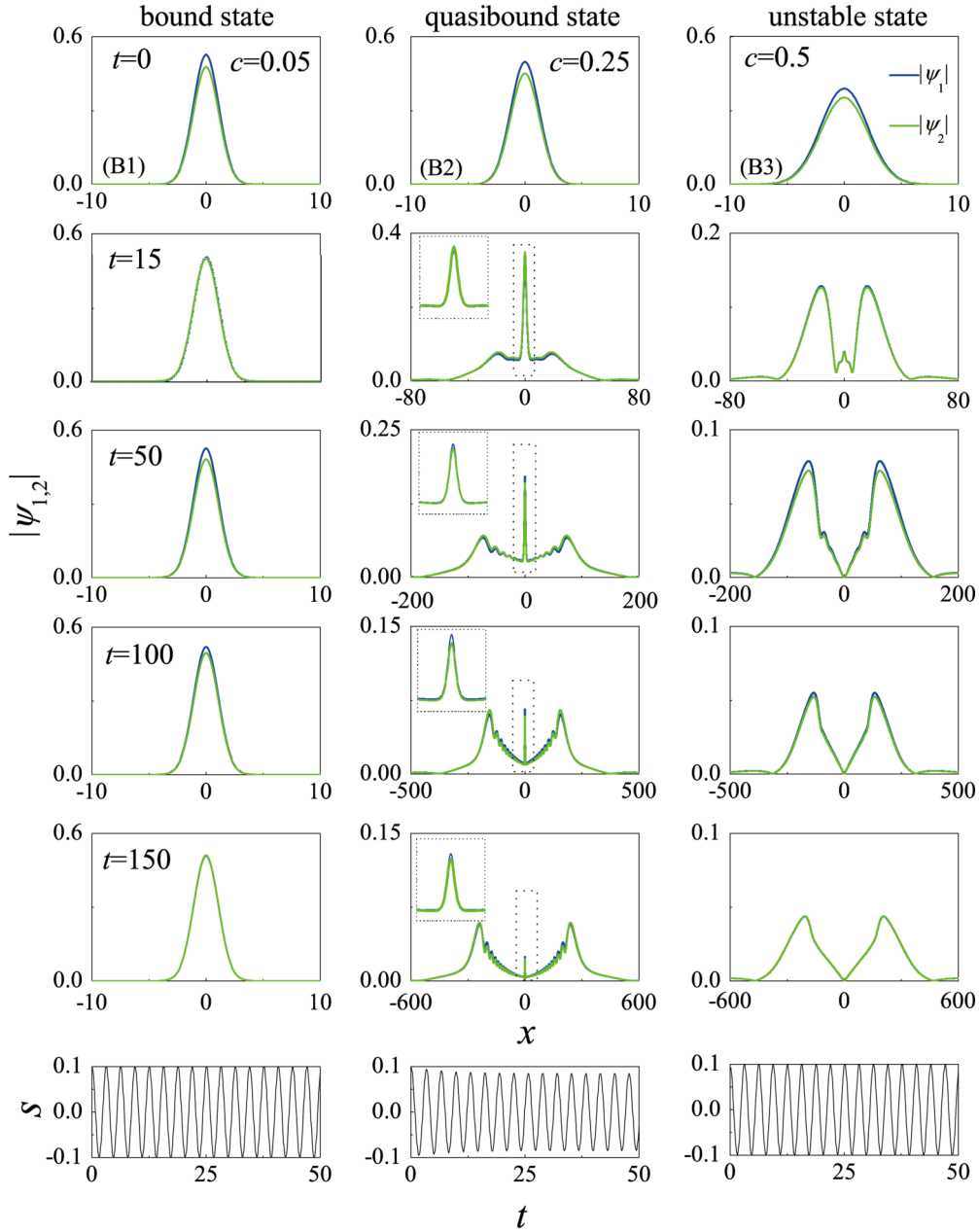


FIG. 5. The time evolution of the wave packets and the spin dynamics corresponds to the cases of B1 (the first column), B2 (the second column), and B3 (the third column) as marked in Fig. 4(a) with $k_L = 0$ (without SOC).

width of the potential well in corresponding cases, so that the wave packet is trapped stably. Equations (7) and (8) always have real solutions under arbitrary value of c . However, these corresponding solutions cannot lead the chemical potential as Eq. (11) tends to 0, thus the vertical lines emerged in Fig. 4.

V. THE TUNNELING AND DIFFUSION DYNAMICS

In order to verify the stability phase diagrams, direct numerical simulation of the dimensionless Gross-Pitaevskii (GP) equation describing the system and the wave packets $|\psi_1|$ and $|\psi_2|$ with their time evolutions of the spin dynamics under the weak excitation in different states as marked by (B1, B2, B3) in Fig. 4(a) are shown in Figs. 6 and 7, and

the case of the condensates without SOC is shown in Fig. 5. Taking the equilibrium states (or after perturbation) as the initial condition [see Eq. (4)], we use the fourth-order Runge-Kutta method to solve $H\Psi = i\dot{\Psi}$ numerically with the time step 0.0001 and space step 0.1, and the corresponding spatial coordinates are calculated to reach 10 000.

The inserts in the second columns of Figs. 5–7 are the enlargements of the corresponding wave packets. Figure 8 is the time evolution of the particle number $\tilde{N}_{j,\sigma}$ ($\tilde{N}_{j,\sigma} = \int_{\sigma} \psi_j^* \psi_j d\sigma$) escaped from the shallow trap of different components along different spatial directions. $j = (1, 2)$ represents the j th component, and $\sigma = (L, R)$ represents the escape direction of atoms; i.e., $\sigma = L(R)$ means atoms escaped from the left (right) side of the well.

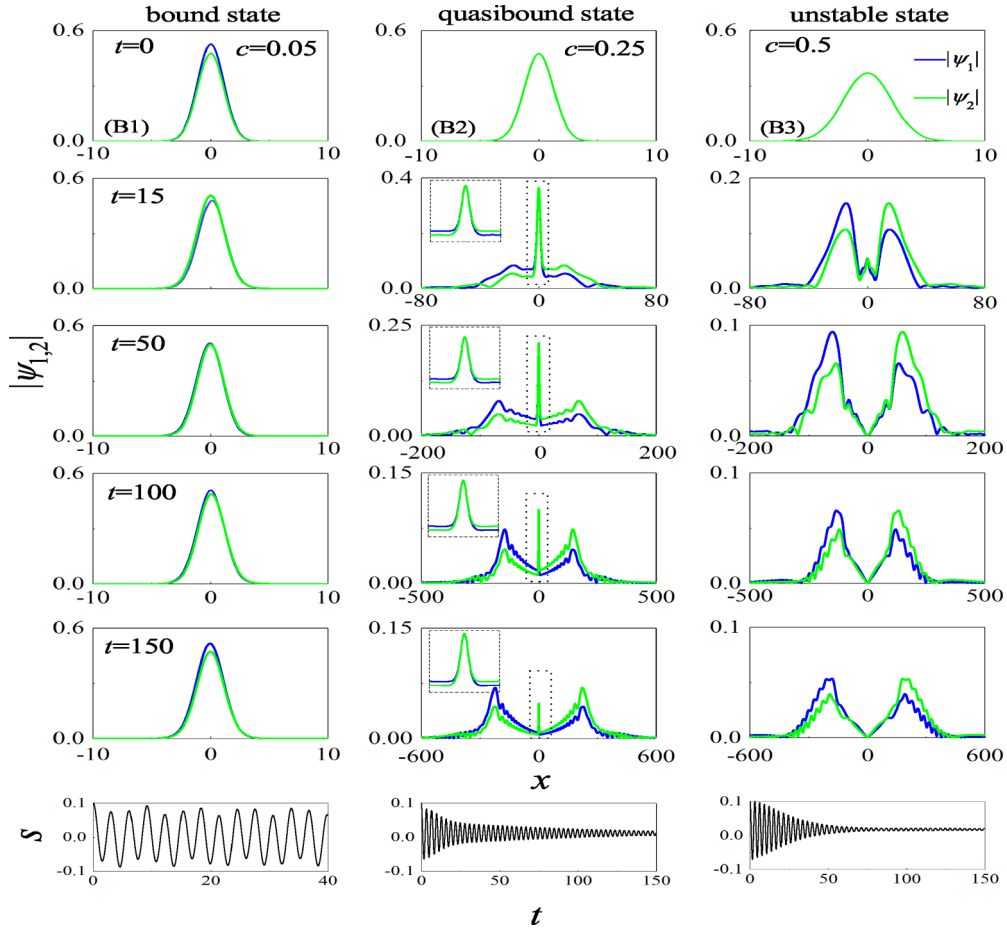


FIG. 6. The time evolution of the wave packets and the spin dynamics corresponds to the cases of B1 (the first column), B2 (the second column), and B3 (the third column) as marked in Fig. 4(a) with $k_L = 0.5$ (in zero-momentum phase).

As is shown in the first columns of Figs. 5–7, the wave packets are stably trapped in the potential well with initial Gaussian form in the bound state for all cases. In the bound state, periodic spin exchange occurs under the weak excitation near the ground state ($\Delta s = 0.1$), and the spin exchange in the plane-wave phase is slowed (i.e., with low spin oscillation frequency) but the spin oscillation amplitude is amplified to $\Delta s = \pm 1$ (see the last rows of the first column in Figs. 5–7). The second columns in Figs. 5–7 illustrate the time evolutions of the wave packets and the spin dynamics in the quasibound state; the wave packets inside the well remain Gaussian form while the atoms of two pseudospin components tunnel out from the potential well asymmetrically in space in the presence of SOC [see Figs. 6 and 7, 8(c), and 8(e)] but symmetrically in space in the absence of SOC [see Figs. 5 and 8(a)]. As is shown in the third columns in Figs. 5–7, when the condensates are in an unstable state, the potential well is too weak to trap the condensates, and the condensates spill out from the top of the potential well asymmetrically in space in the presence of SOC [see also Figs. 8(d) and 8(f)] but symmetrically in space in the absence of SOC [see also Fig. 8(b)] accompanied with the rapid collapse of the wave packets inside the well. That is, in the absence of SOC, Fig. 5 indicates that the tunneling and diffusion behaviors of the two pseudospin components are almost the same; i.e., the wave packets of component ψ_1 and ψ_2 almost coincide, and

the atom clouds of both components tunnel and are diffusive totally symmetrically [see also Figs. 8(a) and 8(b)] in space accompanied with periodic spin oscillations in the bound state, quasibound state, and unstable state (see the last rows in Fig. 5). However, for the cases of condensates with SOC in both quasibound and unstable states (see Figs. 6 and 7), SOC leads to space anisotropic tunneling and escape of the pseudospin components ψ_1 and ψ_2 , and a larger amount of the ψ_1 (ψ_2) component tunnels or escapes along the negative (positive) x direction [see also Figs. 8(c)–(f)]. This would be the results of the additional momentum induced by SOC, which has opposite directions for two pseudospin components [see Eq. (2)]. In addition, when the atoms tunnel out or escape from the well, the atom clouds of both components are diffusive nearly symmetrically in space accompanied with damped spin oscillations in the zero-momentum phase (see the second and third columns in Fig. 6), while the condensates enter into a new spin-polarized state and are diffusive asymmetrically in space in the plane-wave phase (see the second and third columns in Fig. 7); i.e., the diffusion velocity is larger (smaller) in the negative (positive) x direction. The expansion of the wave packet in the positive x direction appears as a quick deceleration with a sharp edge which resembles a form of an effective localization. Figures 5–7 also predict that the tunneling dynamics and diffusion dynamics of the wave packets behave in significant different characters.

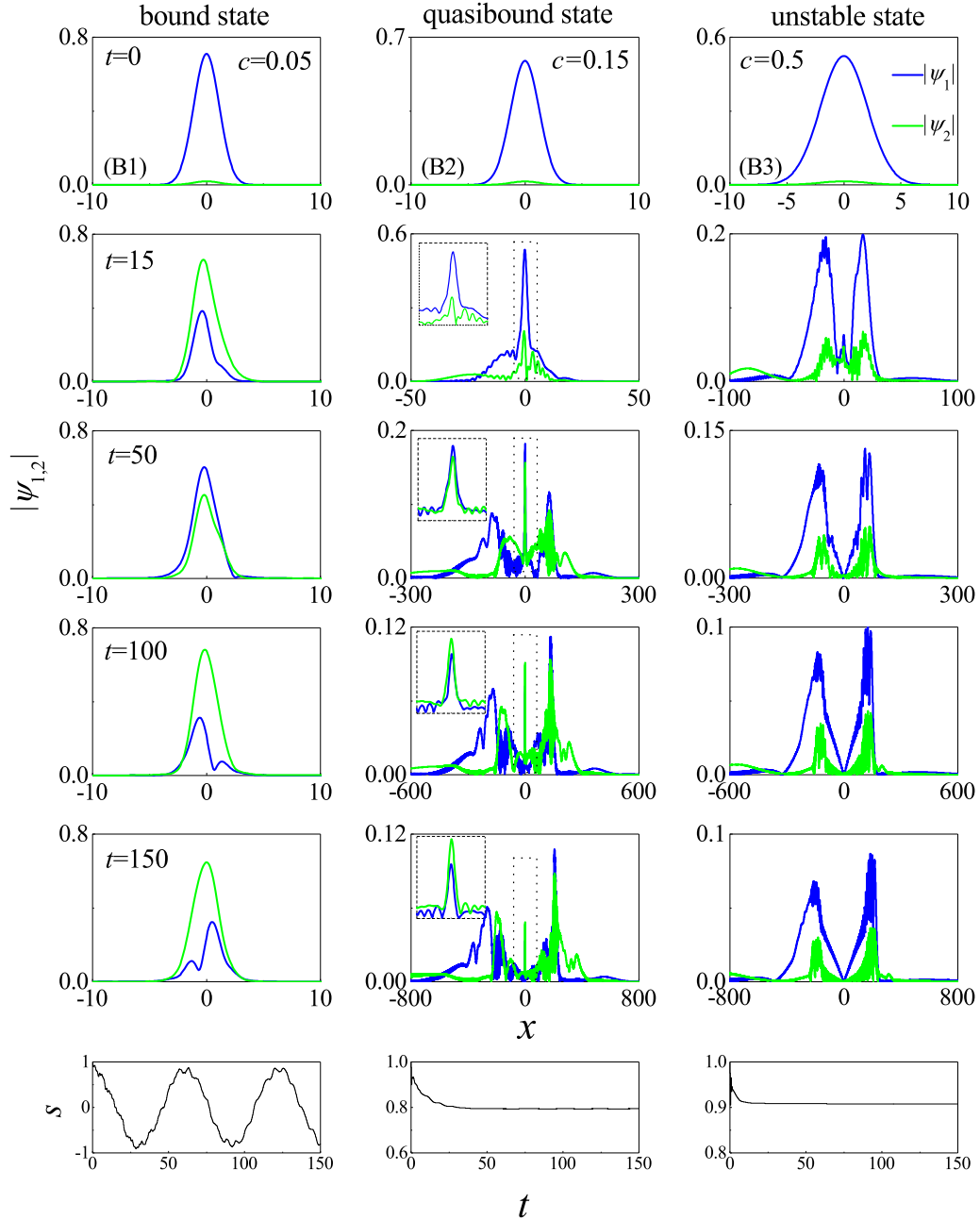


FIG. 7. The time evolution of the wave packets and the spin dynamics corresponds to the cases of B1 (the first column), B2 (the second column), and B3 (the third column) as marked in Fig. 4(a) with $k_L = 3$ (in plane-wave phase).

We note that spin dynamics in different states has different oscillating characters. When the condensates are in the bound state, the wave packets are trapped in the finite potential well stably, and there is no density modulation in this case. Periodic spin oscillations occur under the weak excitation ($\Delta s = 0.1$), and this is known as collective dynamics similar to the collective dynamics in harmonic potential [51]. When the condensates are in the quasibound and unstable state, condensates can tunnel or diffuse outside the finite depth potential well, and the density modulation occurs in this case. The collective dynamics of s are destroyed due to the instability of the system, and the periodic spin oscillations are replaced by the spin polarization; i.e., spin oscillations are damped

(see the second and third columns in Figs. 6 and 7). However, in the absence of spin-orbit coupling ($k_L = 0$), the density modulation and spin oscillations are decoupled, and the density modulation is weak. The wave packets $|\psi_1|$ and $|\psi_2|$ are almost overlapped, the periodic spin exchange caused by Raman coupling Ω also occurs in the quasibound and unstable states (see the second and third columns in Fig. 5).

We introduce the effective mass to illustrate the spatial anisotropic tunneling and diffusion dynamics induced by SOC in the plane-wave phase. It is shown that when the condensates enter into a negative mass region, a marked asymmetry expansion dynamics is observed [35,36]. We obtain the effective mass of the system by using $1/m^* = \partial^2 E / \partial p^2$ in the ground

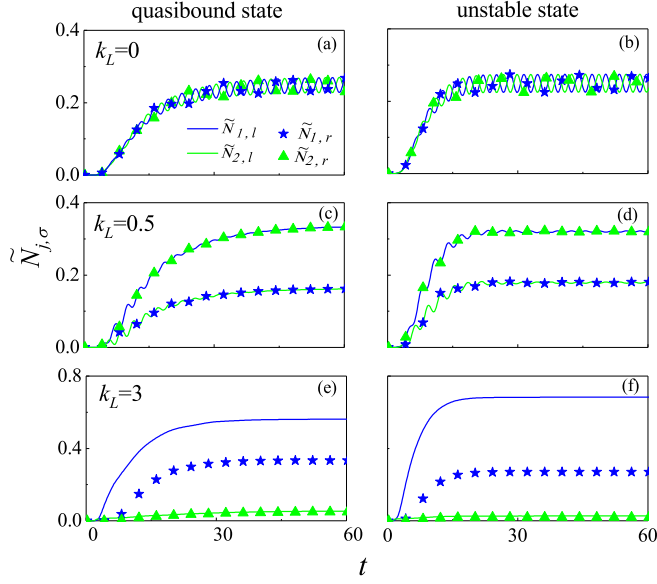


FIG. 8. Time evolution of particle number escaped from the shallow trap of different components along different directions. (a) and (b) correspond to the cases of Fig. 5, (c) and (d) correspond to the cases of Fig. 6, and (e) and (f) correspond to the cases of Fig. 7.

state. Then the effective mass near the phase transition point ($s \rightarrow 0$) has the following form:

$$m^* = -\frac{k_L^2}{k_L^2 - k_{LC}^2}. \quad (12)$$

When $k_L < k_{LC}$, the condensates are in the zero-momentum phase, the effective mass of the ground state m^* is positive, and the diffusion dynamics is symmetry in space (see Fig. 6), while when $k_L > k_{LC}$, the condensates are in plane-wave phase, the effective mass of the ground state m^* is negative, and this leads the spatial anisotropic diffusion dynamics (see Fig. 7).

In order to understand the tunneling and diffusion dynamics more clearly, the variation of the total particle number N inside the well ($N = \int_{-\sqrt{\frac{c}{c}}}^{\sqrt{\frac{c}{c}}} [(\psi_1^* \psi_1 + \psi_2^* \psi_2) dx]$) with time t for different cases shown in Figs. 5–7 is shown in Fig. 9. The escaping rate of the atoms from the potential well is different for the bound, quasibound, and unstable states. The number of atoms in the potential well remains unchanged in the bound state, i.e., condensates do not undergo tunneling or diffusion. In the quasibound state, condensates continue to escape from the potential well, and the particle number in the potential well reduces to 0 for a relatively long time, i.e., tunneling occurs. In the unstable state, the particle number in the potential well decreases to 0 in a very short time, and condensates diffuse and spill over the potential well in this case. As mentioned earlier, the SOC can enhance the stability of the system, however, once the atoms escape from the potential well, i.e., the system deviates from the ground state, k_L (an additional momentum) promotes the diffusion and tunneling weakly, i.e., larger k_L causes relatively obvious tunneling and diffusion rate. Thus, tunneling and diffusion can

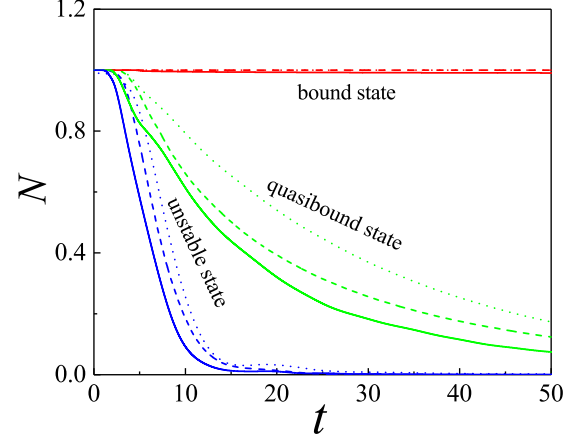


FIG. 9. Time evolution of the total particle number inside the shallow trap for the cases shown in Figs. 5–7. Dotted lines represent $k_L = 0$, dashed lines represent $k_L = 0.5$, and solid lines represent $k_L = 3$.

be more precisely controlled, which plays a significant role in quantum transportation.

VI. SOC (RAMAN COUPLING) INDUCED STABILITY (INSTABILITY) OF THE SYSTEM

The SOC (Raman coupling) induced stability (instability) shown in Fig. 4 can be verified by solving the full GP equation numerically just as in Sec. V (the weak excitation is not considered in this case). Figure 10 (Fig. 11) is the time evolution of the wave packets for the case of D1 (D2) marked in Figs. 4(a) and 4(b) when k_L (Ω) increases, and the inserts in the second columns of Figs. 10 and 11 are the enlargements of the corresponding wave packets. As is shown in Fig. 10, the condensates experience a diffusion

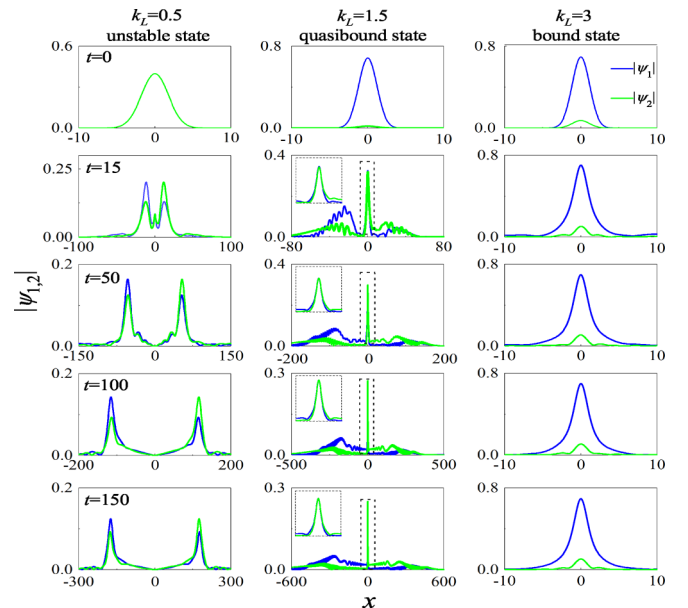


FIG. 10. The time evolution of the wave packets corresponds to the cases of D1 as marked in Fig. 4(a) for different k_L . We set $\Omega = 1$.

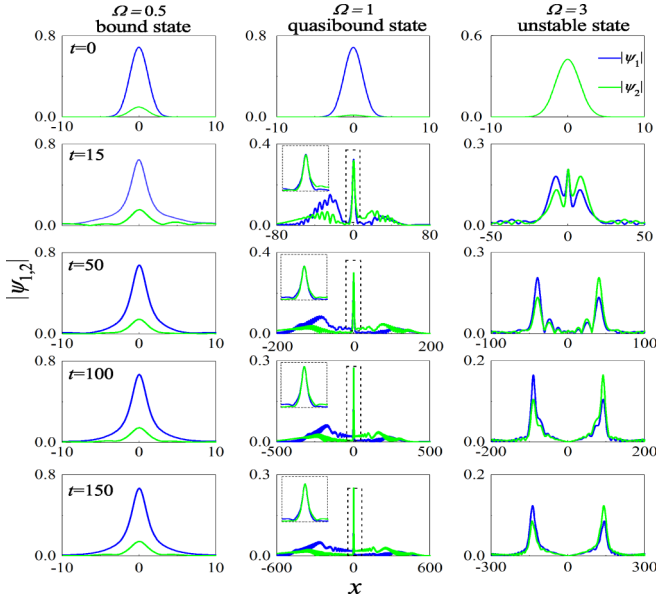


FIG. 11. The time evolution of the wave packets corresponds to the cases of D2 as marked in Fig. 4(b) for different Ω . We set $k_L = 1.5$.

state in the zero-momentum phase, quasibound state in the plane-wave phase, and bound state in the plane-wave phase transitions successively with the increase of k_L under the fixed Ω .

However, Fig. 11 indicates that, for the fixed k_L , when Ω increases, the condensates experience a bound state in the plane-wave phase, a quasibound state in the plane-wave phase, and an unstable diffusion state in the zero-momentum phase transitions successively. Those prove the positive (negative) effect of SOC (Raman coupling) on enhancing the system stability intuitively and confirm the theoretical prediction of Fig. 4. In order to further clarify this mechanism, the effective potential E versus R obtained from Eq. (3) is plotted in Fig. 12.

Figure 12(a) clarifies that the minimum effective potential corresponding to the ground state appears gradually with the increase of k_L under the fixed Ω ; i.e., k_L indeed plays a role in maintaining stability of the system. However, Fig. 12(b) manifests that increasing Ω results in the gradual disappearance of the effective potential's minimum under the fixed k_L ; i.e., Ω indeed plays a role in weakening the stability of the system.

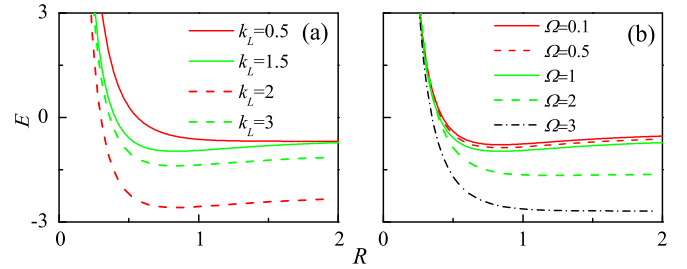


FIG. 12. The effective potential E versus R for the cases D1 and D2 as marked in Fig. 4 with different k_L and Ω .

VII. SUMMARY

In conclusion, we investigate the phase transition and stability of the ground state of SOC-BECs with two pseudospin components trapped in a finite depth potential well by variational method and numerical simulation. The phase transition from the zero-momentum phase to the plane-wave phase still occurs in the finite depth potential well system. The finite depth potential well is beneficial to the phase transition from the plane-wave phase to the zero-momentum phase when interspecies interaction is larger than the intraspecies interaction. The effect of the finite depth potential well on the phase transition becomes significant for larger repulsive interspecies interaction. Importantly, different from the infinite depth harmonic potential well, a metastable state (quasibound state) exists between the bound and unstable diffusion states where tunneling occurs. SOC can enhance the stability of the system, but once the system is far from the ground state, SOC as an external momentum will promote the condensates to escape from the finite depth potential well. Interestingly, SOC results in spatial anisotropic tunneling and diffusion dynamics. The mechanisms and differences between the diffusion and tunneling dynamics are also revealed. This work provides an effective model and method to study quantum tunneling and diffusion dynamics.

ACKNOWLEDGMENTS

This work is supported by the National Natural Science Foundation of China under Grants No. 11764039, No. 11847304, No. 11865014, No. 11475027, No. 11305132, and No. 11274255, by the Natural Science Foundation of Gansu Province under Grant No. 17JR5RA076, and by the Scientific Research Project of Gansu Higher Education under Grant No. 2016A-005.

[1] M. Z. Hasan and C. L. Kane, *Rev. Mod. Phys.* **82**, 3045 (2010).
 [2] D. C. Tsui, H. L. Stormer, and A. C. Gossard, *Phys. Rev. Lett.* **48**, 1559 (1982).
 [3] J. D. Koralek, C. P. Weber, J. Orenstein, B. A. Bernevig, S. C. Zhang, S. Mack, and D. D. Awschalom, *Nature (London)* **458**, 610 (2009).
 [4] J. Wunderlich, B. Kaestner, J. Sinova, and T. Jungwirth, *Phys. Rev. Lett.* **94**, 047204 (2005).

[5] H. A. Engel, E. I. Rashba, and B. I. Halperin, *Handbook of Magnetism and Advanced Magnetic Materials* (Cornell University Library, Ithaca, NY, 2007).
 [6] D. Xiao, M. C. Chang, and Q. Niu, *Rev. Mod. Phys.* **82**, 1959 (2010).
 [7] M. König, S. Wiedmann, C. Brüne, A. Roth, H. Buhmann, L. W. Molenkamp, X. L. Qi, and S. C. Zhang, *Science* **318**, 766 (2007).

- [8] D. Stepanenko and N. E. Bonesteel, *Phys. Rev. Lett.* **93**, 140501 (2004).
- [9] N. Goldman, G. Juzeliūnas, P. Öhberg, and I. B. Spielman, *Rep. Prog. Phys.* **77**, 126401 (2014).
- [10] H. Zhai, *Rep. Prog. Phys.* **78**, 026001 (2015).
- [11] Y. A. Bychkov and E. I. Rashba, *J. Phys. C* **17**, 6039 (1984).
- [12] G. Dresselhaus, *Phys. Rev.* **100**, 580 (1955).
- [13] J. Y. Zhang, S. C. Ji, Z. Chen, L. Zhang, Z. D. Du, B. Yan, G. S. Pan, B. Zhao, Y. J. Deng, H. Zhai, *et al.*, *Phys. Rev. Lett.* **109**, 115301 (2012).
- [14] Y. J. Lin, K. Jiménez-García, and I. B. Spielman, *Nature (London)* **471**, 83 (2011).
- [15] T. L. Ho and S. Zhang, *Phys. Rev. Lett.* **107**, 150403 (2011).
- [16] J. Radic, T. A. Sedrakyan, I. B. Spielman, and V. Galitski, *Phys. Rev. A* **84**, 063604 (2011).
- [17] M. Merkl, A. Jacob, F. E. Zimmer, P. Ohberg, and L. Santos, *Phys. Rev. Lett.* **104**, 073603 (2010).
- [18] L. Salasnich and B. A. Malomed, *Phys. Rev. A* **87**, 063625 (2013).
- [19] Y. V. Kartashov, V. V. Konotop, and D. A. Zezyulin, *Phys. Rev. A* **90**, 063621 (2014).
- [20] A. Tononi, Y. Wang, and L. Salasnich, *Phys. Rev. A* **99**, 063618 (2019).
- [21] Y. V. Kartashov, V. V. Konotop, and F. Kh. Abdullaev, *Phys. Rev. Lett.* **111**, 060402 (2013).
- [22] Y. Zhang, Y. Xu, and T. Busch, *Phys. Rev. A* **91**, 043629 (2015).
- [23] A. L. Fetter, *Phys. Rev. A* **89**, 023629 (2014).
- [24] C. F. Liu, Y. M. Yu, S. C. Gou, and W. M. Liu, *Phys. Rev. A* **87**, 063630 (2013).
- [25] S. Sinha, R. Nath, and L. Santos, *Phys. Rev. Lett.* **107**, 270401 (2011).
- [26] Y. Li, L. P. Pitaevskii, and S. Stringari, *Phys. Rev. Lett.* **108**, 225301 (2012).
- [27] H. Hu, B. Ramachandhran, H. Pu, and X. J. Liu, *Phys. Rev. Lett.* **108**, 010402 (2012).
- [28] C.-F. Liu, H. Fan, Y.-C. Zhang, D.-S. Wang, and W.-M. Liu, *Phys. Rev. A* **86**, 053616 (2012).
- [29] J. Li, Y.-M. Yu, L. Zhuang, and W.-M. Liu, *Phys. Rev. A* **95**, 043633 (2017).
- [30] B. A. Malomed, *Prog. Opt.* **43**, 71 (2002).
- [31] T. Ozawa and G. Baym, *Phys. Rev. Lett.* **109**, 025301 (2012).
- [32] H. Sakaguchi, B. Li, and B. A. Malomed, *Phys. Rev. E* **89**, 032920 (2014).
- [33] Y. C. Zhang, Z. W. Zhou, B. A. Malomed, and H. Pu, *Phys. Rev. Lett.* **115**, 253902 (2015).
- [34] Z. F. Yu, A. X. Zhang, R. A. Tang, H. P. Xu, J. M. Gao, and J. K. Xue, *Phys. Rev. A* **95**, 033607 (2017).
- [35] M. A. Khamehchi, K. Hossain, M. E. Mossman, Y. P. Zhang, T. Busch, M. M. Forbes, and P. Engels, *Phys. Rev. Lett.* **118**, 155301 (2017).
- [36] C. L. Qu, L. P. Pitaevskii, and S. Stringari, *New J. Phys.* **19**, 085006 (2012).
- [37] P. Schlagheck and T. Paul, *Phys. Rev. A* **73**, 023619 (2006).
- [38] L. D. Carr, M. J. Holland, and B. A. Malomed, *J. Phys. B: At. Mol. Opt. Phys.* **38**, 3217 (2005).
- [39] N. Moiseyev, L. D. Carr, B. A. Malomed, and Y. B. Band, *J. Phys. B* **37**, L193 (2004).
- [40] J. L. Qin, *J. Phys. B: At. Mol. Opt. Phys.* **52**, 045002 (2019).
- [41] N. Moiseyev and L. S. Cederbaum, *Phys. Rev. A* **72**, 033605 (2005).
- [42] L. D. Carr and Y. Castin, *Phys. Rev. A* **66**, 063602 (2002).
- [43] D. A. Alcalá, G. Urban, M. Weidemüller, and L. D. Carr, *Phys. Rev. A* **98**, 023619 (2018).
- [44] X. X. Zhao, D. A. Alcalá, M. A. McLain, K. Maeda, S. Potnis, R. Ramos, A. M. Steinberg, and L. D. Carr, *Phys. Rev. A* **96**, 063601 (2017).
- [45] S. Potnis, R. Ramos, K. Maeda, L. D. Carr, and A. M. Steinberg, *Phys. Rev. Lett.* **118**, 060402 (2017).
- [46] Y. V. Kartashov, V. V. Konotop, D. A. Zezyulin, and L. Torner, *Phys. Rev. A* **94**, 063606 (2016).
- [47] Y. V. Kartashov, V. V. Konotop, D. A. Zezyulin, and L. Torner, *Phys. Rev. Lett.* **117**, 215301 (2016).
- [48] P. P. Beličev, G. Gligorić, J. Petrovic, A. Maluckov, L. Hadžievski, and B. A. Malomed, *J. Phys. B: At. Mol. Opt. Phys.* **48**, 065301 (2015).
- [49] T. L. Ho, *Phys. Rev. Lett.* **81**, 742 (1998).
- [50] T. Ohmi and K. Machida, *J. Phys. Soc. Jpn.* **67**, 1822 (1998).
- [51] Z. F. Yu and J. K. Xue, *Europhys. Lett.* **121**, 20003 (2018).